Journal of Materials Chemistry A

Accepted Manuscript

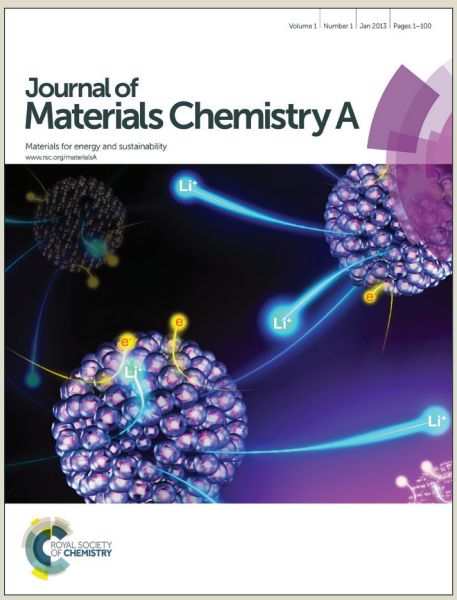

ROYAL SOCIETY OF CHEMISTRY

www.rsc.org/materialsA

Journal of Materials Chemistry A

Dynamic Article Links ►

Cite this: DOI: 10.1039/c0xx00000x

www.rsc.org/xxxxxx

COMMUNICATION

Carbonized poly(vinylidene fluoride)/graphene oxide with three-dimensional multiscale-pore architecture as advanced electrode materials

Mianqi Xue,[*a] Dong Chen,[a] Xusheng Wang,[b] Jitao Chen[*b] and G. F. Chen[a]

Received (in XXX, XXX) Xth XXXXXXXXX 20XX, Accepted Xth XXXXXXXXX 20XX
DOI: 10.1039/b000000x

A low-cost, mass-produced, dry-gel-based method for fabricating graphene based electroactive material relevant to energy storage has been reported. This technique combines thermal decomposition of carbon-based materials for ultrami-cropores/micropores-forming and freeze dry of graphene gels for mesopores/macropores creating. As-fabricated pore-rich carbon material shows electrochemical performances with superior characteristics of stabilization, specific capacitance and rate capability, demonstrating its great potential application in clean energy.

Electrochemical double-layer capacitors (EDLCs), with the superior rate performance (compared to lithium-ion batteries), are based on predominantly electrostatic storage of electrical energy and are determined by the combination of a high-surface-area activated electrode material as well as a nanoscopic charge separation at the electrode–electrolyte interface[1]. Graphene, with high intrinsic electrical conductivity, accessible and defined pore structure, good resistance to oxidative processes, high temperature stability and real high-surface-area, ensures that the relevant EDLCs exhibit high energy and power densities, and also ultra-rate capability[2-7]. Although the development of graphene supercapacitors is very encouraging for the possibility of substituting commercial activated carbon based EDLCs, there are still issues which must be addressed before pushing graphene-based supercapacitor into practical application, especially the high irreversible capacitance (which leading to low specific capacity and unusable cyclic property) [8-10].

The high irreversible capacitance which can be considered as an increase of inert components in graphene-based supercapacitor is mainly caused by the two-dimensional stack of graphene and the reduced conductivity of electrons or protons arising therefrom. It is imperative for researchers to develop an easy and powerful method to make graphene-based materials inherit excellent properties of graphene and possess three-dimensional (3D) support to solve the stack and reunion[11]. Presently, three are mainly two solutions to this issue: reducing the number of defects and/or choosing a better electrolyte[12-15]. In practical application, both solutions are effective in microsystem, but one of the real options that might actually solve the problem is mostly outside mainstream debate in the conventional devices[16]. On the other hand, carbonization of polymers or their composites are noticed to be used as porous carbon electrodes in EDLCs for the introducing of ultramicropores (<0.7 nm) and micropores (<2 nm), besides their high surface area and relatively good electrical conductivity[17,18]. Following these principles and the advantages of graphene in supercapacitor as mentioned above, here we report a low-cost, mass-produced electroactive material for high performance EDLCs based on the carbonization of poly(vinylidene fluoride)/graphene oxide (CPVDFG). As-fabricated CPVDFG possesses 3D multiscale-pore architectures and ultrahigh-surface-area, leading to a large specific capacity of more than 200 F/g, high charge/discharge currents even at 50 A/g and only a minor capacitance loss after 9000 cycles.

During the experiment, graphene oxide (GO) sheets were synthesized by a modified Hummer method using natural graphite powder, which reported elsewhere[19]. GO aqueous solution was fabricated by dispersing the GO sheets in water after a two-step sonication. An atomic force microscopy (AFM) image (Figure 1a) clearly shows the GO nanosheets with different diameter (ranging from several hundred nanometers to several micrometers) but uniform thickness around 1~2 nm. The GO aqueous solution was then treated by standard separation and centrifugation multistep process to remove the larger and smaller GO sheets. To demonstrate the purification effect, GO was self-assembled to form a thin layer (with the thickness around 15 nm) on a piece of silica wafer. AFM image in Figure 1b shows the continuous and classy wrinkled surface feature of the GO nanolayer. This represents good interface but few agglomeration, impurities and defects. The GO nano-film was then reduced by hydrazine vapor. The obtained reduced graphene oxide (rGO) shows similarity in film morphology and thickness to the original

GO thin film. The rGO nano-film is electrically continuous, exhibiting ohmic behavior (with linear current–voltage curve). It should be noted that the using of hydrazine vapor reduction rather than thermal reduction is mainly due to the difficulty of morphology remaining. Figure 1c shows the Raman spectrum (532 nm) of the as-fabricated GO nano-film at room temperature. D and G peaks are observed at ~1345 and ~1589 cm^{-1} which correspond to the E_{2g} mode observed for sp^2 carbon domains and edges and/or defects of the sp^2 domains, respectively. Poly(vinylidene fluoride) (PVDF) solutions with different concentration of GO ranging from 0.25 wt% to 5 wt% were used for fabricating PVDF/GO gel[20,21] which were then freeze dried for 24 h after ageing for 4 days and solvent exchanging in water for 5 days to produce dried porous materials. Figure 1d is the scanning electron microscopy (SEM) image of the resulting PVDF/GO dried porous gels. The porous dry-gels are constructed by flaky nano-materials and few microspheres. It can still be found the characteristic peak of graphene in the Raman spectrum of PVDF/GO as shown in Figure 1e.

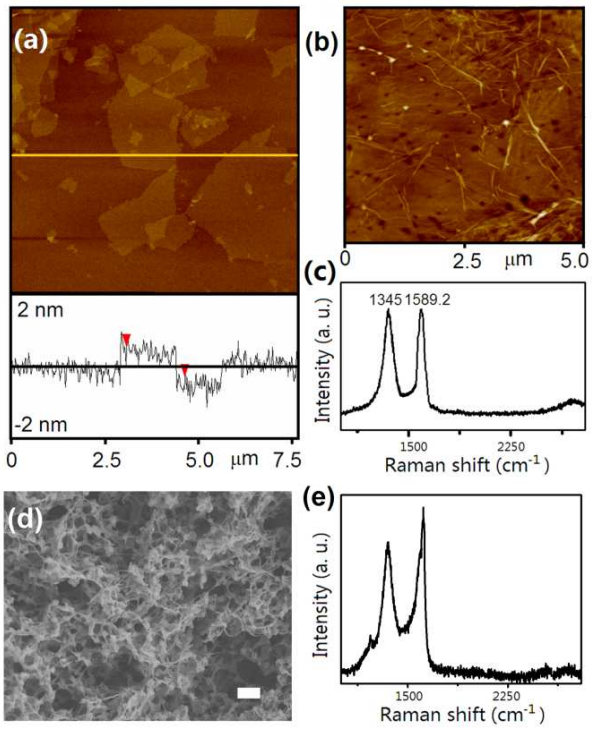

Figure 1. (a) AFM image of the GO nanosheets without purification. The bright yellow line arising from the overlapping of graphene nanosheets shows the uniform thickness of nanosheets as ~1.1 nm. (b) AFM image of the self-assembly thin film of purified GO nanosheets. The continuous and classy-wrinkled surface of the rGO layer shows non-agglomeration and good purification of as-prepared GO. (c) The Raman spectrum of the GO nanofilm. (d) SEM image of the PVDF/GO, the scale bar: 1 μm. (e) The Raman spectrum of the PVDF/GO.

The as-fabricated PVDF/GO was then put into a tube furnace and heated to the carbonization temperature (600-1000 ℃ at 5 ℃/min) under nitrogen protection. The morphology of the as-fabricated CPVDFG shows some changes after carbonization (Samples with the carbonization temperature at 950 ℃ were used for the following issues in this communication.) Figure 2a shows a higher magnification of the CPVDFG image, indicating the slightly thinner thickness of flaky nano-materials and more obvious holes after carbonization than PVDF/GO showed in Figure 1d. Similar to the PVDF/GO, there is no difference between the image of the cross-section of CPVDFG and Figure 2a. The inset of Figure 2b shows the edges of flaky nanosheets in CPVDFG. A close look at a piece of flaky nanosheet by high-resolution transmission electron microscopy (HRTEM) suggests that the as-prepared CPVDFG contains graphene with different layer numbers (labelled by parallel lines), graphite-like nanosheets (in the rectangle) and amorphous carbon (in the oval). The intensive distribution of graphene shows the high levels of graphene content (can up to 5 wt%). The graphene shows a slightly curved appearance, which is strikingly different from other graphene prepared without oxidation step[22]. The graphite-like nanosheets are probably from the reunion of GO and the carbonization of part of PVDF with better crystallinity. The amorphous carbon is mainly produced by the carbonization of PVDF.

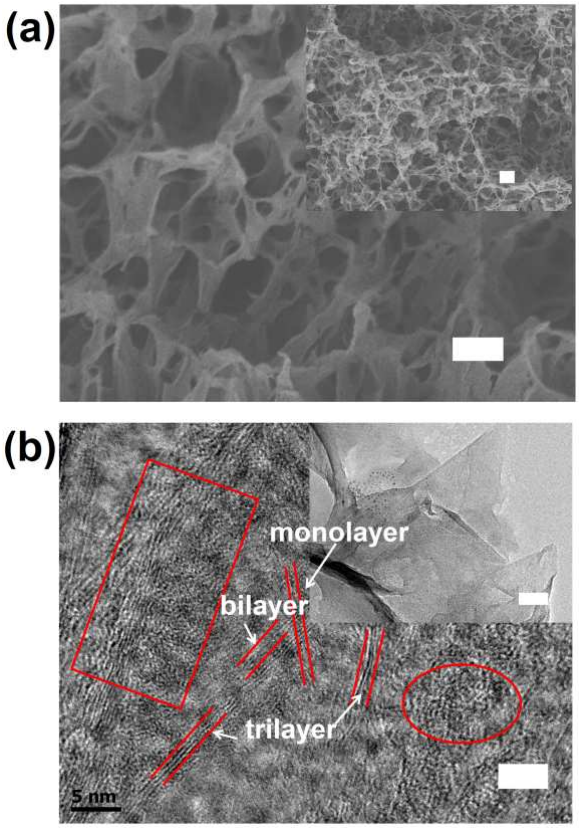

Figure 2. (a) Magnified view of the CPVDFG. Inset: SEM of CPVDFG. Scale bar: 100 nm, inset is 1 μm. (b) HRTEM images of CPVDFG. Inset: TEM of CPVDFG. Scale bar: 5 nm, inset is 100 nm.

Figure 3a shows cyclic voltammetry (CV) curves of the CPVDFG electrodes at various scan rates of 10, 50, 100, and 500 mV/s in 6 M KOH recorded in the potential range of –0.1 and 0.6 V, respectively. The CV curves of the CPVDFG electrode exhibit a relatively ideal rectangular shape and near mirror-image current response on voltage reversal, and no obvious redox peak was observed, indicating a typical EDLC capacitive behavior and excellent electrochemical reversibility. In a parallel experiment, carbonized PVDF (CPVDF) without GO was fabricated as electrode material. The specific capacitance of porous CPVDFG

and CPVDF at different charge/discharge current densities are compared in Figure 3b and Figure s2. The result shows that the CPVDFG possesses higher specific capacitance values and better maintenance capability at high current density (even at 50 A/g) compared to CPVDF. The specific capacitance is calculated from galvanostatic charge/discharge curves. The CPVDFG can provide a larger specific capacitance of 204.8 F/g at 0.85 A/g between 0 and 1 V. These curves indicate that the CPVDFG has higher power density and better high-rate discharge characteristic than CPVDF. Moreover, the porous CPVDFG electrode exhibits a superior charge/discharge cycle characteristics, with only a minor capacitance loss (less than 3%) observed after 9000 cycles at 5A/g, as shown in Figure 3c.

The high specific capacitance of CPVDFG may be ascribed to the ultramicropores and micropores (ranging from 0.5 to 5 nm, measured by gas adsorption–desorption isotherms, similar to other reports[17,18,20]) which are created from the releasing of hydrogen fluoride (HF) in the thermal decomposition step (accounts for the vast majority of the micropores) and the abundant various deficiencies in graphene (mainly provides mesopores, has little contribution for porous carbon). The released HF in this step needs to be cleared and managed in time. The surface area (BET surface area of the CPVDFG can reach as high as more than 900 m^2/g) is well enhanced by these kinds of pores which are large enough for the ion transport. The existence of ultramicropores may limits the high-rate ability to some degree, but the introducing of defects and doping ions (by introducing of graphene oxide and gel structure) can provide mesopores even macropores, leading the better high-rate discharge characteristic than CPVDF[23,24]. The synergistic effect in these porous materials can be attributed to the following four points. First, these mesopores and macropores are favorable for the rapid diffusion of electrolytes. Second, abundant and homogeneous distribution of graphene with outstanding electrical conductivity in the CPVDFG (as shown in TEM images) allows the efficient electronic channels and adsorption/desorption efficiency of surface charge[25]. Third, the high mechanical strength of graphene with large aspect ratio can enhance the stability of porous materials and prevent the collapse and destruction of the multiscale-pore structures. Fourth, the presence of heteroatoms such as oxygen can considerably contribute to an additional pseudo-capacitance as well as improve the wettability with the electrolyte[17]. All these synergistic effects of multiscale pores and the maintenance of the good properties of graphene make it a reality that CPVDFG delivers a high specific capacitance, superior rate performance and even perfect stability.

In summary, this communication demonstrates a facile and low-cost procedure for fabricating electroactive material for EDLCs by carbonization of PVDF/GO dry-gel. The as-fabricated CPVDFG shows outstanding electrochemical performance with superior characteristics of stabilization, specific capacitance and rate capability. Our study clearly reveals that there are abundant multiscale pores and graphene-like nanostructures in those CPVDFG for improving the electrochemical performance of supercapacitors. The technique we describe here is a universal and mass-produced method for fabricating 3D multiscale-pore structures, especially in graphene-based composite materials, since the thermal decomposition during the carbonization can provide ultramicropores and micropores, the introducing of graphene and gel structure can provide mesopores even macropores. We also believe that such materials will be an option for future practical applications of graphene-based devices, not only the supercapacitor, but also conductive ink, antistatic, electromagnetic-interference shielding, and gas barrier applications[12].

This work was supported by the Natural Science Foundation of China (21304002), Qinghai Province Science and Technology program (2012-G-Y28, 2013-G-Q12A-1) and Shenzhen Science and Technology Innovation Commission (JCYJ20120829170028561).

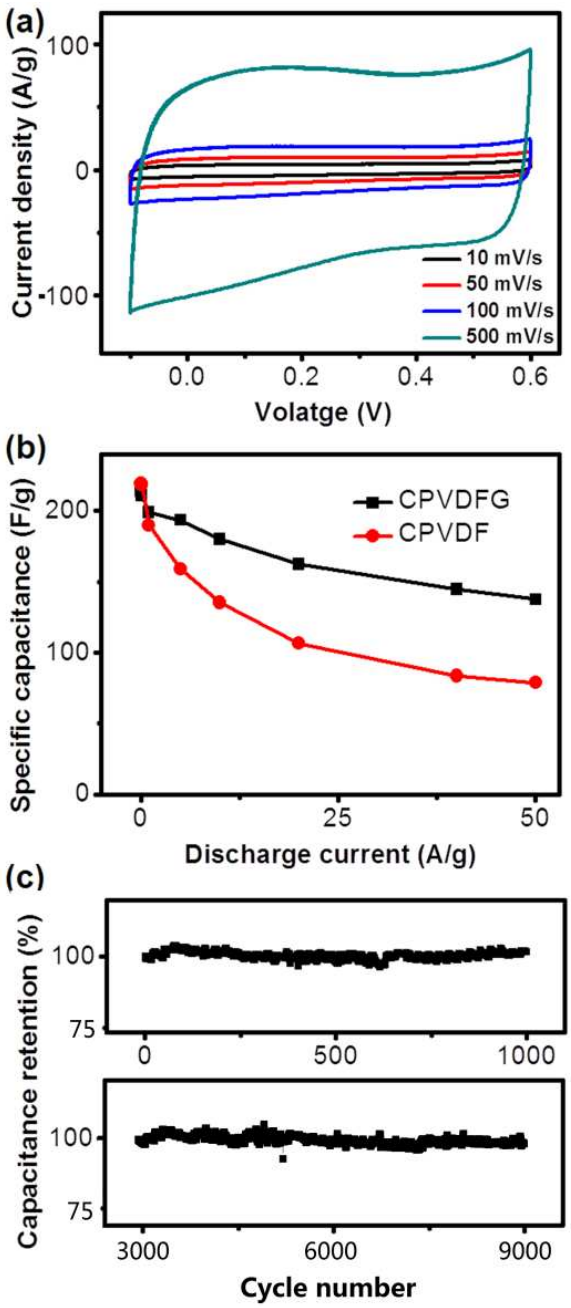

Figure 3. Electrochemical characteristics of CPVDFG. (a) CV curves of CPVDFG at different scan rates. (b) Specific capacitance of CPVDFG and CPVDF in supercapacitor calculated from the corresponding discharge curve in galvanostatic charge/discharge curves at different charge/discharge current densities ranging from 0.01 to 50 A/g. (c) Cycle performance of the CPVDFG electrode with the current density at 5 A/g.

Notes and references

[a]*Institute of Physics and Beijing National Laboratory for Condensed Matter Physics, Chinese Academy of Sciences, Beijing 100190, China. E-mail: xuemq@iphy.ac.cn*
[b]*Beijing National Laboratory for Molecular Sciences, College of Chemistry and Molecular Engineering, Peking University, Beijing 100871, China. E-mail: chenjitao@pku.edu.cn*
† Electronic Supplementary Information (ESI) available: [Detailed information about experimental methods]. See DOI: 10.1039/b000000x/

1. Wang, H.; Köster, T. K. J.; Trease, N. M.; Segalini, J.; Taberna, P. L.; Simon, P.; Gogotsi, Y.; Grey, C. P. *J. Am. Chem. Soc.* **2011**, *133*, 19270-19273.
2. Zhu, Y. W.; Murali, S.; Stoller, M. D.; Ganesh, K. J.; Cai, W.; Ferreira, P.; Pirkle, A.; Wallace, R.; Cychosz, K.; Thommes, M.; Su, D.; Stach, E. A.; Ruoff, R. S. *Science* **2011**, *332*, 1537-1541.
3. El-Kady, M. F.; Strong, V.; Dubin, S.; Kaner, R. B. *Science* **2012**, *335*, 1326-1330.
4. Xu, M.; Liang, T.; Shi, M.; Chen, H. *Chem. Rev.* **2013**, *113*, 3766-3798.
5. Cui, C.; Qian, W.; Yu, Y.; Kong, C.; Yu, B.; Xiang, L.; Wei, F. *J. Am. Chem. Soc.* **2014**, *136*, 2256-2259.
6. Yang, X. W.; Cheng, C.; Wang, Y. F.; Qiu, L.; Li, D. *Science* **2013**, *341*, 534-537.
7. a) Wang, H. L.; Liang, Y. Y.; Gong, M.; Li, Y. G.; Chang, W.; Mefford, T.; Zhou, J. G.; Wang, J.; Regier, T.; Wei, F.; Dai, H. J. *Nat. Commun.* **2012**, *3*, 917; b) Zhu, J.; Yang, D.; Yin, Z.; Yan, Q.; Zhang, H. *Small* **2014**, *10*, 3480-3498; c) Yu Y.; Sun, Y.; Cao, C.; Yang, S.; Liu, H.; Li, P.; Huang, P.; Song, W. *J. Mater. Chem. A* **2014**, *2*, 7706-7710.
8. Chen, Z. P.; Ren, W. C.; Gao, L. B.; Liu, B. L.; Pei, S. F.; Cheng, H. M. *Nat. Mater.* **2011**, *10*, 424-428.
9. Jha, N.; Ramesh, P.; Bekyarova, E.; Itkis, M. E.; Haddon, R. C. *Adv. Energy Mater.* **2012**, *2*, 438-444.
10. Xu, Z.; Gao, C. *Nat. Commun.* **2011**, *2*, 571.
11. Song, J. Y.; Wang, Y. Y.; Wan, C. C. *J. Power Sources* **1999**, *77*, 183-197.
12. Novoselov, K. S.; Fal'ko, V. I.; Colombo, L.; Gellert, P. R.; Schwab, M. G.; Kim, K. *Nature* **2012**, *490*, 192-200.
13. Presser, V.; Heon, M.; Gogotsi, Y. *Adv. Funct. Mater.* **2011**, *21*, 810-833.
14. Butler, S. Z.; Hollen, S. M.; Cao, L. Y.; Cui, Y.; Gupta, J. A.; Gutiérrez, H. R.; Heinz, T. F.; Hong, S. S.; Huang, J.; Ismach, A. F.; Johnston-Halperin, E.; Kuno, M.; Plashnitsa, V. V.; Robinson, R. D.; Ruoff, R. S.; Salahuddin, S.; Shan, J.; Shi, L.; Spencer, M. G.; Terrones, M.; Windl, W.; Goldberger, J. E. *ACS Nano* **2013**, *7*, 2898-2926.
15. Niu, Z.; Zhang, L.; Liu, L.; Zhu, B.; Dong, H.; Chen, X. *Adv. Mater.* **2013**, *25*, 4035-4042.
16. Vickery, J. L.; Patil, A. J.; Mann, S. *Adv. Mater.* **2009**, *21*, 2180-2184.
17. a) Xu, B.; Hou, S.; Duan, H.; Cao, G.; Chu, M.; Yang, Y. *J. Power Sources* **2013**, *228*, 193-197; b) Chung, S. H.; Manthiram, A. *Adv. Mater.* **2014**, *26*, 1360–1365.
18. Xu, B.; Hou, S.; Chu, M.; Cao, G.; Yang, Y. *Carbon* **2010**, *48*, 2812-2814.
19. a) Xue, M.; Li, F.; Zhu, J.; Song, H.; Zhang, M.; Cao, T. *Adv. Funct. Mater.* **2012**, *22*, 1284-1290; b) Li, F.; Xue, M.; Ma, X.; Zhang, M.; Cao, T. *Anal. Chem.* **2011**, *83*, 6426-6430; c) Liu, H.; Gao, J.; Xue, M; Zhu, N.; Zhang, M; Cao, T. *Langmuir* **2009**, *25*, 12006-12010.
20. Zha, D.; Mei, S.; Wang, Z.; Li, H.; Shi, Z.; Jin, Z. *Carbon* **2011**, *49*, 5166-5172.
21. a) Eswaraiah, V.; Balasubramaniam, K.; Ramaprabhu. S. *Nanoscale* **2012**, *4*, 1258-1262; b) Tang, H. X.; Ehlert, G. J.; Lin, Y. R.; Sodano, H. *Nano Lett.* **2012**, *12*, 84-90.
22. Xue, M.; Chen, G.; Yang, H.; Zhu, Y.; Wang, D.; He, J.; Cao, T. *J. Am. Chem. Soc.* **2012**, *134*, 6536-6539.
23. Wu, Z.-S.; Sun, Y.; Tan, Y.-Z.; Yang, S.; Feng, X.; Müllen, K. *J. Am. Chem. Soc.* **2012**, *134*, 19532-19535.
24. Kajdos, A.; Kvit, A.; Jones, F.; Jagiello, J.; Yushin, G. *J. Am. Chem. Soc.* **2010**, *132*, 3252-3253
25. a) Bonanni, A.; Ambrosi, A.; Chua, C. K.; Pumera, M. *ACS Nano* **2014**, *8*, 4197-4204; b) Zhang, B.; Fan, L.; Zhong, H.; Liu, Y.; Chen, S. *J. Am. Chem. Soc.* **2013**, *135*, 10073-10080; c) Ma, X.; Zhao, D.; Xue, M.; Wang, H.; Cao, T. *Angew. Chem., Int. Ed.* **2010**, *49*, 5537-5540.

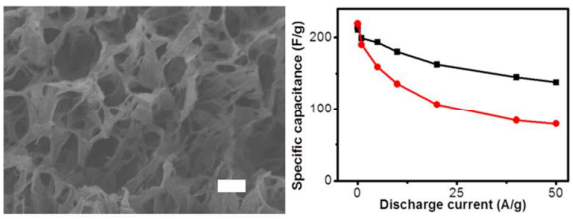

A low-cost, mass-produced, dry-gel-based method has been developed for fabricating high performance graphene-based electroactive material with 3D multiscale-pore architecture.